MICROBIOLOGY

Biogenic formation of amorphous carbon by anaerobic methanotrophs and select methanogens

Kylie D. Allen[1], Gunter Wegener[2,3], D. Matthew Sublett Jr[4], Robert J. Bodnar[4], Xu Feng[5], Jenny Wendt[2], Robert H. White[1]*

Elemental carbon exists in different structural forms including graphite, diamond, fullerenes, and amorphous carbon. In nature, these materials are produced through abiotic chemical processes under high temperature and pressure but are considered generally inaccessible to biochemical synthesis or breakdown. Here, we identified and characterized elemental carbon isolated from consortia of anaerobic methanotrophic archaea (ANME) and sulfate-reducing bacteria (SRB), which together carry out the anaerobic oxidation of methane (AOM). Two different AOM consortia, ANME-1a/HotSeep-1 and ANME-2a/c/Seep-SRB, produce a black material with similar characteristics to disordered graphite and amorphous carbon. Stable isotope probing studies revealed that the carbon is microbially generated during AOM. In addition, we found that select methanogens also produce amorphous carbon with similar characteristics to the carbon from AOM consortia. Biogenic amorphous carbon may serve as a conductive element to facilitate electron transfer, or redox active functional groups associated with the carbon could act as electron donors and acceptors.

INTRODUCTION

Most of the elements found on Earth are processed through many different oxidation states as a result of both abiotic and biotic reactions. The oxidation state of carbon varies widely in nature, ranging from methane (−4) to carbon dioxide (+4). One of these states is pure elemental carbon (oxidation state of 0), which occurs in highly ordered crystalline forms, such as graphite and diamond, or as amorphous "black" carbon that lacks crystalline structure (*1*, *2*). Crystalline carbon is naturally produced under high heat and pressure in Earth's crust and in the upper mantle, while amorphous carbon is found primarily in coal and charcoal produced by incomplete combustion of biomaterials as well as in carbonaceous chondrite meteorites (*3*, *4*).

The different forms and amounts of elemental carbon are influenced mainly by abiotic geochemical processes. However, some evidence exists for the biological degradation of elemental carbon. For example, pyrogenic black carbon in soil is degraded on a centennial time scale facilitated by both abiotic processes and by microbial oxidation (*5*). The rate of microbial degradation depends on the degree of thermal alteration of the carbon to generate biochemically accessible sites (*6*). The bacterial aerobic catabolism of amorphous carbon was first reported by Potter in 1908 (*7*), and more recent studies support microbially facilitated degradation of black carbon (*8*, *9*), but the associated biochemical mechanism remains unclear. In addition, fungi have been shown to oxidize diamond-like carbon films (*10*), and the fungus *Neosartorya fischeri* is proposed to metabolize coal via an oxidative enzyme (*11*). Despite the evidence for biodegradation of elemental carbon, the biological production of elemental carbon appears to have never been reported.

Methane, the most reduced form of carbon, is produced and consumed in anaerobic environments by methanogenic and methanotrophic archaea, respectively. Methanogens are widespread anaerobes that perform methanogenesis with various substrates including H_2/CO_2, small methylated compounds, and acetate (fig. S1) (*12*). Methanogenesis is one of the first forms of energy metabolisms to arise on Earth and is responsible for the production of over a billion tons of methane each year, which accounts for at least 70% of global methane emissions (*12*, *13*). Related to methanogens are anaerobic methanotrophic archaea (ANME) that carry out the anaerobic oxidation of methane (AOM) to CO_2 using a reverse methanogenesis pathway (fig. S1) (*14*). AOM is an essential component of the global methane budget and has a substantial role in controlling the amount of methane released from marine sediments (*15*, *16*). There are four major clades of ANME—ANME-1 (*17*) (subclusters a and b), ANME-2 (*18*) (subclusters a, b, and c), ANME-2d (*19*) (more recently referred to as Candidatus Methanoperedenaceae) (*20*), and ANME-3 (*21*)—which inhabit different ecological niches and differ in their physiology (*15*, *21*, *22*). Most ANME exist in syntrophic consortia with sulfate-reducing bacteria (SRB), which use reducing equivalents obtained from AOM for the reduction of sulfate to sulfide (*23*–*26*).

Here, we report on the identification and characterization of amorphous carbon produced by two different AOM enrichment cultures. The AOM50 culture (cultured at 50°C) derived from the gas-rich, hydrothermal vents of the Guaymas Basin and is dominated by consortia of ANME-1a and HotSeep-1 partner bacteria (*24*, *27*, *28*). The AOM20 culture (cultured at 20°C) derived from cold seeps at the Nile deep sea fan and is dominated by ANME-2a/c and Seep-SRB partner bacteria (*28*, *29*). Further, we investigated several methanogenic species and confirmed the production of amorphous carbon in *Methanocaldococcus jannaschii*, *Methanococcus maripaludis*, and *Methanosarcina barkeri*.

RESULTS

Initial inspection of black matter present in AOM cultures

Both the AOM50 and the AOM20 cultures are dominated by large microbial consortia, formed either by ANME-1a and HotSeep-1 partner bacteria or by ANME-2a/c and Seep-SRB partner bacteria, respectively. The consortia exhibited amber-like color, which is due

[1]Department of Biochemistry, Virginia Tech, Blacksburg, VA 24061, USA. [2]MARUM, Center for Marine Environmental Sciences, University Bremen, D-28359 Bremen, Germany. [3]Max Planck Institute for Marine Microbiology, D-28359 Bremen, Germany. [4]Department of Geosciences, Virginia Tech, Blacksburg, VA 24061, USA. [5]Department of Chemistry, Virginia Tech, Blacksburg, VA 24061, USA.
*Corresponding author. Email: rhwhite@vt.edu

to the high abundance of cytochromes produced by the consortial members (*23*, *24*) (Fig. 1, A and B). The AOM biomass includes abundant opaque black matter and lucent larger crystals. The black components appear within and around the AOM biomass but also float in the medium. To study both components, AOM biomass was harvested, and the pellets were resuspended in deionized water. This procedure lysed most cells but left a dark grainy residue. Microscopic observations of material derived from ANME-1a/HotSeep-1 samples under higher magnification showed two types of solid materials, including large clear crystals and abundant black spheres with diameters of 2.5 to 4.5 μm (Fig. 1C). The sample from ANME-2a/c/Seep-SRB consortia showed a higher abundance of dark material (Fig. 1D). The clear crystals, especially evident in material from ANME-1a/HotSeep-1 samples (Fig. 1C), were identified as crystals of magnesium phosphates that are formed by excess phosphate in the culture medium (described more below and in the Supplementary Materials).

To investigate the origin of the black matter, we analyzed uninoculated and spent media from both AOM cultures, which showed no sign of black matter in the absence of cells. To determine which organism in the consortia was responsible for the production of the black matter, we examined pure cultures of the AOM partner bacterium, *Candidatus* Desulfofervidus auxilii, a member of the HotSeep-1 clade (*30*). Cell pellets from this organism grown on hydrogen gas as the electron donor did not contain the black material observed in AOM consortia. Because sulfate-dependent ANME are obligate syntrophs, they cannot be analyzed in pure culture. However, the absence of black matter in pure cultures of *Ca.* D. auxilii suggests that the ANME are responsible for the generation of the black matter in the consortia.

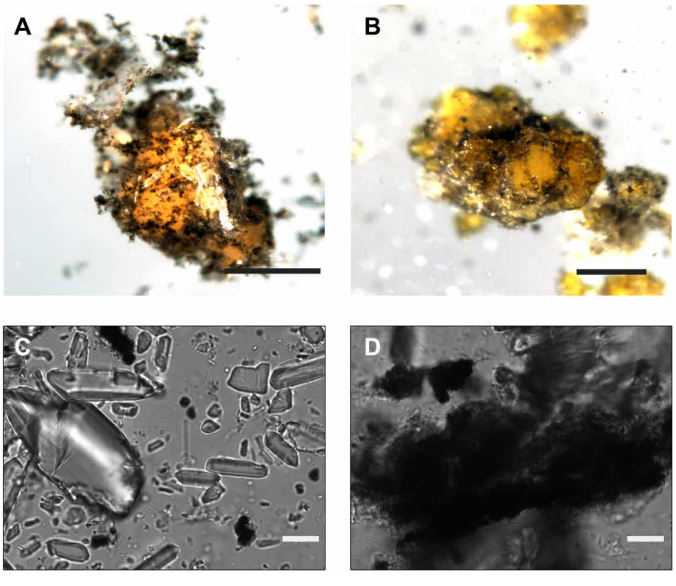

Fig. 1. Light microscopy of intact and lysed AOM biomass. Top: Micrographs of nonfixed active AOM biomass from (**A**) ANME-1a/HotSeep-1 and (**B**) ANME-2a/c/Seep-SRB. Scale bars, 200 μm. Each of the flocks contains several million of cells. The amber-like color of the active cultures is due to the high abundance of cytochromes produced by the consortial members. The black material is found within and attached to the AOM biomass but also floating in the medium. Bottom: The material present in biomass of (**C**) ANME-1a/HotSeep-1 and (**D**) ANME-2a/c/Seep-SRB after harvesting, freezing, and resuspending in deionized water. Scale bars, 10 μm. All cells have lysed in (C) and (D).

Chemical treatment and reactions of AOM biomass components

To resolve the chemical nature of the black matter, we further aimed to enrich and isolate this material from various cultures (Table 1). The heating of cell pellets in 1 M NaOH removed most proteins and other cellular components in the soluble fraction, while the black matter remained as an insoluble pellet. Subsequent treatment of the black pellet with 1 M HCl at 100°C removed most minerals from the sample. FeS was completely removed in this treatment, but FeS_2 remained (see the Supplementary Materials). The FeS_2 was removed by heating the sample in 70% nitric acid for 1 hour. Last, an extended treatment of the remaining black pellet with nitric acid and HCl for 2 days at 100°C resulted in the solubilization of the black matter to generate a dark brown solution. Together, the behavior of the black material upon various chemical treatments led us to the hypothesis that the material was elemental carbon, which is a highly unreactive substance—insoluble in water, most acids and bases, and organic solvents. The solubilization of elemental carbon in the concentrated nitric acid and HCl over an extended period of time occurs through functionalization of the carbon surfaces with hydroxyl, ketone, and ether groups (*31*).

To address whether the elemental carbon could be produced via abiotic chemical reactions, an anoxic solution of sodium bicarbonate, Fe(II), and HS^- was heated at 100°C for 5 days. This process produced a black precipitate composed of FeS and/or FeS_2. This material easily dissolved in 70% nitric acid; thus, it did not contain amorphous carbon (see the Supplementary Materials). We additionally tested whether the black matter represented scoring of the rubber stoppers used to seal anaerobic culture bottles, yet chemical and spectroscopic analysis clearly excluded rubber as a possible source of the black carbon identified in the AOM cultures (see discussion in the Supplementary Materials and fig. S2).

Analysis of AOM culture components by scanning electron microscopy/energy dispersive x-ray spectroscopy

To further investigate the composition of the bulk black matter derived from AOM consortia, cell pellets were analyzed by scanning electron microscopy/energy dispersive x-ray spectroscopy (SEM/EDS). SEM images of desiccated biomass from ANME-2a/c/Seep-SRB consortia showed two main types of solid materials, including large crystals (gray) and small particles (bright white) (Fig. 2A). Bulk elemental analysis by EDS of a large crystal (area 1) gave 72.6 atomic % (at %) O, 16.0 at % Mg, and 9.4 at % P, which is consistent with the stoichiometry of the magnesium phosphate phase bobierrite [$Mg_3(PO_4)_2$•$8H_2O$] that was further identified by Raman spectroscopy (see the Supplementary Materials). EDS analysis of a small bright particle (area 2) showed 15.3 at % Fe and 29.6 at % S, which matches the stoichiometry for FeS_2 and indicates that pyrite is present in the extracted solid phase.

After removing the magnesium phosphate crystals from the sample by dissolving with 1 M HCl, SEM images showed a mixture of small bright particles and dark rounded structures grouping together (Fig. 2B). The small particles were confirmed by EDS to contain mostly FeS_2 (area 2, 28.9 at % Fe, 47.5 at % S) that were not dissolved by the HCl treatment. The EDS elemental analysis of the large rounded structures (area 1) showed 90.0 at % carbon,

Table 1. Summary of cell pellet appearance before and during the procedure for isolating amorphous carbon from the different organisms studied here.

Organism	Growth substrate/ Electron acceptor	Color of cell pellet	Pellet color after NaOH treatment*	Pellet color after HCl treatment†	Confirmation of elemental carbon‡
ANME-1a/HotSeep-1	CH_4/SO_4^{2-}	Black	Black	Black	+
ANME-2a/c/Seep-SRB	CH_4/SO_4^{2-}	Black	Black	Black	+
Ca. Desulfofervidus auxilii (HotSeep-1)	H_2/SO_4^{2-}	Gray	Pellet almost gone and gray	No pellet observed	–
Methanocaldococcus jannaschii	H_2/CO_2	Black	Black	Mixture of black and white specks	+
Methanococcus maripaludis	H_2/CO_2	Tan with black specks	Black	Black	+
Methanococcus maripaludis	Formate	Tan with black specks	Tan	Tan	+
Methanococcus vannielii	H_2/CO_2	Black	Black and white layers	White	–
Methanosarcina barkeri	Acetate	Dark tan	Black	Black	+
Methanosarcina thermophila (TM1)	Acetate	Black	Tan with black specks	White	–
Methanosarcina acetivorans	Methanol	Tan	Blue gel with a few small black spots	No black	–
Methanospirillium hungateii	H_2/CO_2	Black	Black	Gray	–
Methanoculleus thermophilus	H_2/CO_2	Black	White	White	–
Escherichia coli	LB	Tan	White	White	–

*1 M NaOH at 100°C. †1 M HCl at 100°C. ‡The presence of elemental carbon was confirmed in the final purified samples by Raman Spectroscopy. In samples with originally black cell pellets where elemental carbon was not identified, the black color is likely due to the presence of FeS. The *Methanospirillium hungateii* sample had too much background fluorescence in the sample to confirm the presence of carbon.

0.8 at % sulfur, and 0.3 at % iron, indicating that this material is primarily elemental carbon with some pyrite. These results support the presence of elemental carbon in AOM cultures and suggest that the black particles observed by light microscopy (Fig. 1) were partially composed of elemental carbon.

Analysis of the black matter isolated from AOM cultures by Raman spectroscopy

We used Raman spectroscopy to analyze the black material remaining after treatment of the cell pellets with NaOH to remove most proteins and HCl to remove most minerals (Table 1). The interaction between the laser and the black material during long collection times with unfiltered laser power altered the carbon structure or removed carbonaceous material entirely from the analytical volume (Fig. 3, A to C). Thus, it was necessary to collect the spectra as quickly as possible and filter the laser power at the sample to minimize destruction of the analyte, which resulted in low-intensity spectra. Two different black pellets (sample 1 and sample 2 in Fig. 3) were analyzed from ANME-1a/HotSeep-1 consortia. Both exhibited broad Raman peaks at ~1350 and ~1580 cm^{-1} (Fig. 3D), representing the D (disorder/defect) and the G (graphite) bands, respectively, the features of elemental carbon materials (*32*, *33*). The relative intensities and shapes of the D and G bands provide a metric for assessing the level of order (crystalline carbon) compared to disorder (amorphous carbon) (*34*). The nearly equal intensities of the D and G bands observed for the black material in ANME-1a/HotSeep-1 samples (Fig. 3D) and ANME-2a/c/Seep-SRB samples (fig. S3A) are comparable to Raman spectra for disordered graphite and amorphous carbon (*33*). In addition, both samples do not contain the Raman 2D band at approximately 2680 cm^{-1} indicative of graphene. Some of the carbon-containing particles from ANME-1a/HotSeep-1 cultures were associated with residual phosphate minerals, as evidenced by the phosphate peak located at ~980 cm^{-1} in the sample 1 trace in Fig. 3D. This signal was not produced from the black material but, rather, from the surrounding phosphate mineral that was included in the laser sampling volume. In sample 2, no phosphate peak appeared in the spectrum of the black matter (Fig. 3D, middle spectrum). The clear mass in sample 2 showed evidence of carbon destruction by the laser (Fig. 3C) but still has characteristics of elemental carbon based on the Raman spectrum (Fig. 3D, top spectrum). Notably, none of the samples showed evidence of carbonate minerals, which would exhibit Raman bands at much lower wave numbers (*35*). Overall, the Raman spectra of the black matter from AOM cultures confirm the presence of carbonaceous material with spectral characteristics most consistent with amorphous carbon.

Elemental and chemical analysis of the black matter from AOM cultures by XPS

X-ray photoelectron spectroscopy (XPS) is a widely used technique that provides elemental and chemical state information on the surface of solid materials. Surface elemental analysis of the black pellets from ANME-1a/HotSeep-1 and ANME-2a/c/Seep-SRB consortia resulting after treatments with NaOH and HCl showed ~64 at % C, ~6 at % N, ~21 s O, and negligible amounts of Fe and S

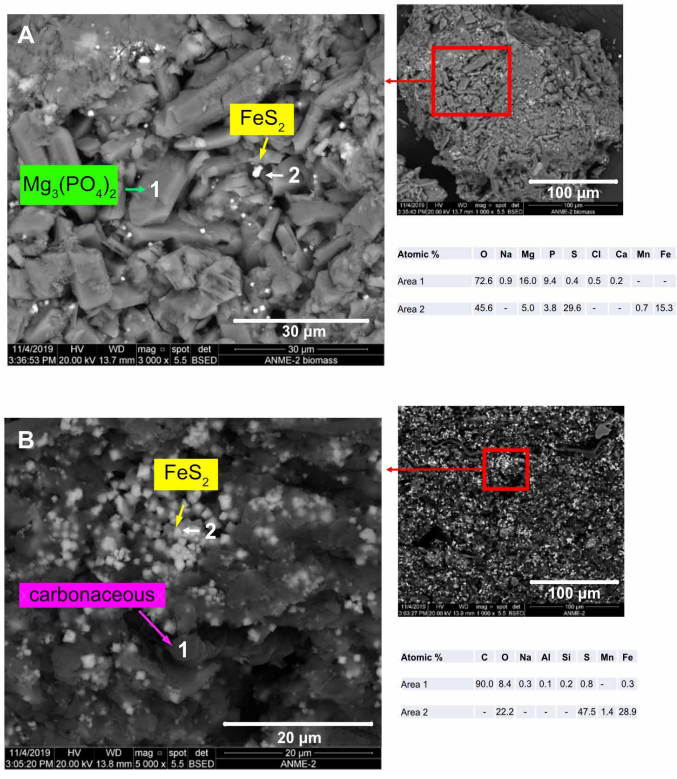

Fig. 2. SEM/EDS of solid materials obtained from AOM cultures. Here, the ANME-2a/c/Seep-SRB culture (Fig. 1, B and D) was analyzed. (**A**) Desiccated biomass showing large crystals of magnesium phosphate and small bright particles consisting of mostly FeS_2. A minor amount of carbon was detected, but the magnesium phosphate crystals dominate this sample. (**B**) After removal of magnesium phosphate by dissolving it in HCl, carbonaceous spheres (larger dark areas) were observed as well as FeS_2 particles (smaller light areas). EDS analysis revealed that the carbon spheres are 90 atomic % (at %) carbon and 0.3 at % iron. Nitrogen is insensitive in EDS and thus was not included in the quantitation.

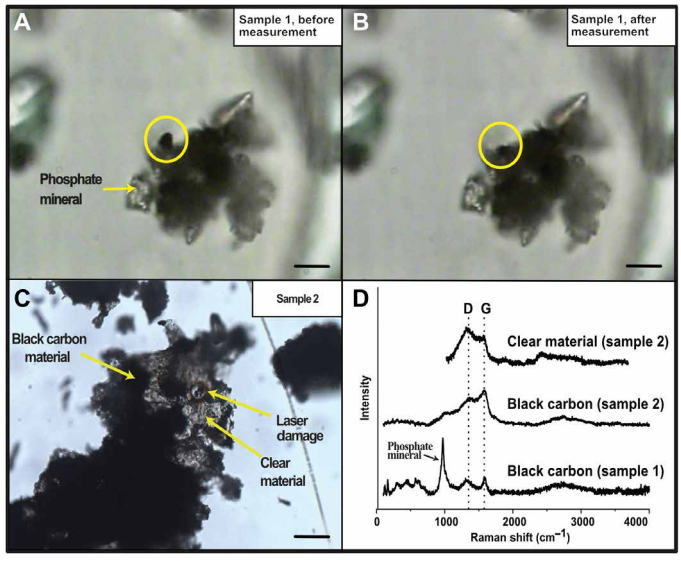

Fig. 3. Raman spectroscopic characterization of the black material in ANME-1a/HotSeep-1 cultures. (**A** to **C**) Photomicrographs of the two different samples analyzed showing laser damage that resulted in low-intensity spectra. Scale bars, ~20 μm. (**D**) Raman spectra showing characteristic D and G bands corresponding to elemental carbon. The sharp peak at ~1000 cm^{-1} in the bottom spectrum is due to the phosphate mineral with which this particular black particle was associated. Excitation was at 514 nm.

(Table 2). An etched sample, revealing the nature of the material in the subsurface of the sample, showed ~79 at % C, ~4 at % N, ~3 at % O, ~8 at % S, and 7 at % Fe, indicating that the bulk of the sample is composed of carbon (Table 2). The C1s spectrum resulting from the surface of the isolated elemental carbon (Fig. 4A) was deconvoluted to reveal ~60% C─C//C═C/C─H, ~28% C─O/C─N, and ~12% C═O/O─C─O. The ANME-2a/c/Seep-SRB carbon shows a similar composition (fig. S3B). These spectral characteristics are primarily due to remaining bound proteins on the surface of the black pellet (discussed more below). The etched sample lacked any evidence of carbon bonded to heteroatoms based on the main well-resolved peak at 285 eV (Fig. 4B), indicating that the bulk of the sample contained elemental carbon. In some cases, sp^2 versus sp^3 bonded carbon can be distinguished from the C1s spectrum (*36*), but often, the difference in peak position is too small to reliably resolve the different carbon bonding types. Thus, to determine whether the carbon was sp^2 or sp^3, the first derivative C KLL XPS spectra of the same samples (surface versus etched) were obtained. The surface of the black pellet showed primarily sp^3 carbon (Fig. 4C, D parameter of 13 eV), whereas the C KLL XPS spectrum from the etched sample (Fig. 4D) revealed that the majority of the bulk carbon was sp^2 as evidenced by the D parameter of 19 eV (*37*).

On the basis of the XPS data, the carbon samples seemed to contain surface-bound molecules, especially proteins and/or peptides that hindered the collection of chemical information from underlying amorphous carbon or other components. All proteins have a basic molecular formula with the ratios of C, H, N, O, and S as $C_{1.00}H_{1.56}N_{0.28}O_{0.29}S_{0.01}$ (*38*). Because XPS does not detect hydrogen atoms, this should produce an average hydrogen-free elemental composition for proteins of $C_{1.00}N_{0.28}O_{0.29}S_{0.01}$, which would correspond to 62.8% C, 17.6% N, and 18.8% O after removing hydrogen from the molecular formula. This is comparable to the measured values of C, N, and O on the surface of the amorphous carbon from AOM cultures (Table 2), which supports the idea that protein is bound to the surface of the carbon samples and thus contributes to the surface chemical information collected by XPS. To validate this conclusion, an XPS depth profile of the black carbon–containing pellet isolated from ANME-1a/HotSeep-1 was obtained (Fig. 4E). XPS sputter depth profiling uses an argon-ion beam to etch layers of the sample surface so that subsurface information can be revealed. During ion etching, at % of O/N/Si/F quickly decreased to minimum values, whereas at % carbon increased from ~63% to ~80%. In addition, Fe and S increased to substantial and steady values. These results support the postulation that the surface of the black particle is coated with proteins, while the subsurface contains primarily carbon with some FeS_2.

Quantitative assessment of amorphous carbon in AOM cultures

To estimate the amount of amorphous carbon produced per mass of cells in AOM cultures, we extracted 15.8 mg of dried ANME-2a/c/Seep-SRB biomass to yield a black pellet of ~0.5 mg (see Materials and Methods for complete isolation procedure). Thus, the original dried cell pellet composed of ~3.2% amorphous carbon by weight.

Table 2. Elemental composition derived from XPS analysis of black pellets resulting after NaOH and HCl treatments. On the basis of the surface composition data, the surface of the black pellets is covered with residual protein. The etched samples reveal primarily carbon as the major component of the black pellet. Data are reported as atomic % (at %).

Sample	C	N	O	F	Na	Mg	Al	Si	P	S	Cl	Ca	Fe	Co	Zn	Br
Surface composition																
ANME-1a/ HotSeep-1	64.6	6.1	20.7	0.8	–	–	–	6.8	–	0.9	–	–	0.2	–	–	–
ANME-2a/c/ Seep-SRB	64.3	7.1	22.1	–	2.0	–	–	3.5	–	0.8	–	0.1	0.2	–	–	–
M. maripaludis	66.5	7.8	21.1	–	–	0.1	0.1	1.9	0.6	1.1	0.3	0.1	–	0.4	–	–
M. jannaschii	75.4	5.3	17.4	–	–	–	–	1.0	0.4	0.1	0.4	–	–	–	–	–
M. barkeri	80.2	3.6	14.0	–	–	–	–	0.4	0.3	0.7	0.5	–	–	0.4	–	–
Etched samples/bulk composition																
ANME-1a/ HotSeep-1	78.7	4.5	2.7	–	–	–	–	–	–	7.5	–	–	6.7	–	–	–
M. maripaludis	75.6	1.8	12.5	–	–	1.1	2.0	3.3	0.9	0.9	0.3	–	–	1.6	–	–
M. jannaschii	93.0	3.3	1.5	–	–	–	–	0.3	0.8	0.5	0.5	–	–	0.1	–	–
M. barkeri	93.5	1.6	2.9	–	–	–	–	0.2	0.1	0.7	0.4	–	–	0.6	–	–

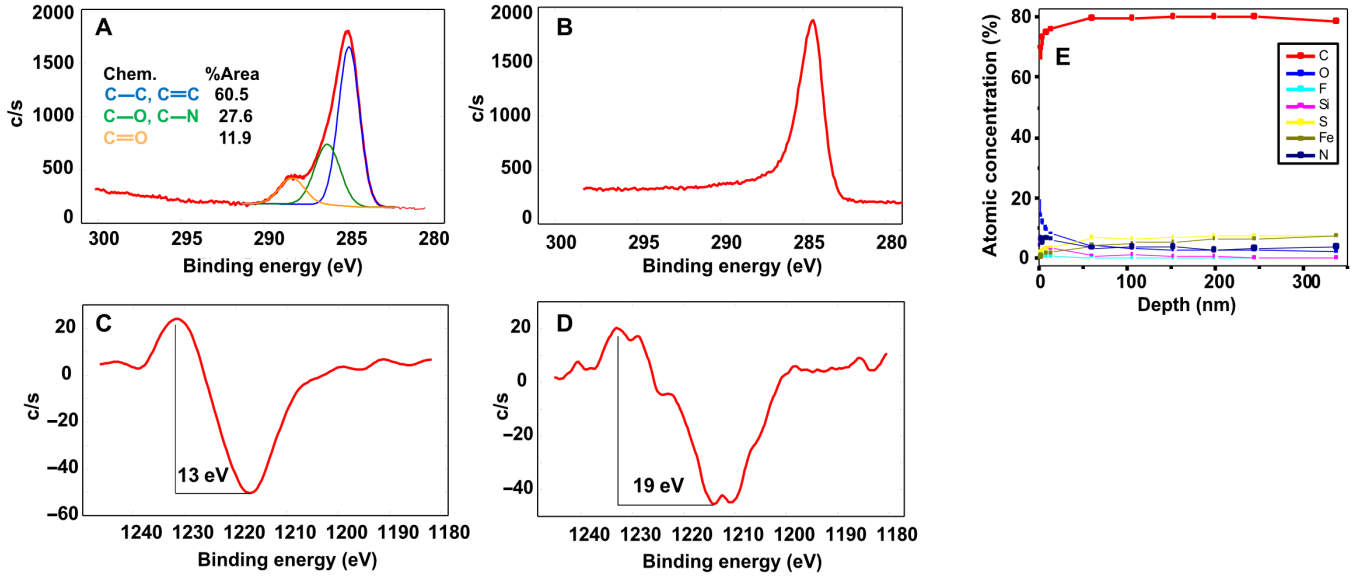

Fig. 4. XPS analysis of black material in ANME-1a/HotSeep-1 cultures. (**A**) The C1s XPS spectrum of the surface of the carbon pellet. (**B**) The C1s XPS spectrum of the etched/subsurface of the carbon pellet, showing primarily carbon-carbon bonds. (**C**) The first derivative C KLL spectrum of the surface of the carbon pellet indicates sp^3 carbon due to proteins on the surface. (**D**) The first derivative C KLL spectrum of the etched sample, indicating primarily sp^2 carbon (D parameter of 19 eV) below the surface of the black pellet. (**E**) XPS sputter depth profile indicates that the black carbon pellet is coated with proteins because of large amounts of nitrogen, while the subsurface of the particle contains up to 80% carbon and smaller amounts of iron and sulfur.

In terms of quantifying the amount of amorphous carbon produced per amount of biomass, this number is underestimated because the dried biomass is also composed of precipitated media components. Further, the final black pellet also contains some residual proteins (see above), which also complicates the quantitation.

Natural isotopic composition of amorphous carbon from AOM cultures

To gain insight into the origin of the amorphous carbon identified in AOM consortia, its stable carbon isotopic compositions were measured (Table 3). Residual proteins were not completely removed

Table 3. Carbon isotopic compositions of amorphous carbon samples isolated from ANME-1a/HotSeep-1 consortia and *M. maripaludis* compared to the reference samples in the bottom three rows. The original carbon isotopic compositions of DIC and methane were −6 and −41‰, respectively. VPDB, Vienna Pee Dee belemnite.

Sample type	$\delta^{13}C$ (‰ vs. VPDB)
ANME-1a/HotSeep-1, sample 1*	−61.0
ANME-1a/HotSeep-1, sample 2*	−60.1
M. maripaludis grown on $H_2 + CO_2$	−31.8
Protein from *M. maripaludis* grown on $H_2 + CO_2$	−35.2
Norit (commercial activated carbon)	−25.0
Acetanilide	−27.4

*The first two samples represent two different measurements of the same isolated black carbon pellet.

from the carbon; hence, the obtained $\delta^{13}C$ values include their isotope signal. On the basis of the carbon-to-nitrogen ratios in the XPS elemental composition measurements (Table 2), we estimate that ~70% of the carbon in the samples is the amorphous carbon, and the remaining is from proteinaceous carbon. The $\delta^{13}C$ values of amorphous carbon from ANME-1a/HotSeep-1 cultures was about −60 per mil (‰), indicating strong ^{13}C depletion representative of biomolecules and total biomass of AOM consortia (*17*, *39*).

Incorporation of ^{13}C-DIC and $^{13}CH_4$ into amorphous carbon by active AOM cultures

To establish the carbon source of the amorphous carbon produced by AOM consortia, ANME-1a/HotSeep-1 cultures were grown for specific time intervals with 5% $^{13}CH_4$ or 5% ^{13}C–dissolved inorganic carbon (DIC)–labeled medium with or without methane as the energy source. Exact isotope composition of both carbon species was determined and used for calculations. At the end of the experiment, carbon isotopic composition of total biomass carbon (TBC) and amorphous carbon was determined (for all data see table S1). Values were transformed into formed TBC or amorphous carbon as fraction (%) of the respective stocks (Fig. 5; see Materials and Methods for calculations). The stable isotope incubations revealed that 16% of the TBC and 5% of the amorphous carbon formed from DIC within 20 days (Fig. 5A). In the same time interval, 3.6% of total carbon and 1.2% of amorphous carbon were produced from CH_4 (Fig. 5B). In the absence of methane, only negligible amounts of DIC were transformed into biomass (Fig. 5C). These experiments show that AOM produces both TBC and amorphous carbon from DIC, but only if methane is provided as energy source. The small amount of $^{13}CH_4$ assimilation argues for an assimilation of catabolically produced ^{13}C-DIC. This is consistent with previous studies showing that ANME archaea and their partner bacteria assimilate primarily DIC as opposed to methane into their biomass (*40*, *41*).

Analysis of proteins bound to the amorphous carbon from AOM cultures

The XPS data indicated that protein was present on the surface of the isolated black material. Proteins are known to readily bind to many different forms of carbon, including carbon nanotubes (*42*) and amorphous carbon (*43*). To confirm the presence of protein, the black material from AOM cultures was subjected to acid hydrolysis, and the production of amino acids was confirmed by thin-layer chromatography with ninhydrin detection (see the Supplementary Materials). To determine whether any specific protein was bound to the amorphous carbon that could be involved in its function or formation, the carbon pellet was heated with SDS loading buffer to extract proteins on the surface of the pellet, followed by SDS–polyacrylamide gel electrophoresis (PAGE) analysis of the resulting soluble material. After staining the gel with Coomassie, the extracted sample showed a heavy smear of proteins and peptides. Two areas of this gel were removed, digested with trypsin, and analyzed by matrix-assisted laser desorption/ionization mass spectrometry (MALDI-MS) to identify the proteins present. At least 100 different proteins were identified (top 20 hits are listed in table S2). The top hit was methyl-coenzyme M reductase, which is one of the most highly abundant proteins in ANME and methanogens. Because of this wide range of proteins identified, they are likely not specifically associated with the carbon but, instead, are adventitiously bound.

Evidence of iron associated with amorphous carbon from AOM cultures

To obtain some information about the molecular structure of the amorphous carbon in AOM cultures, an amorphous carbon sample from the ANME-1a/HotSeep-1 culture was analyzed by MALDI-MS. Two major ions corresponding to carbon structures associated with iron were observed, one at mass/charge ratio (m/z) 932.3 (intensity, 2.7×10^4) and a less intense ion at m/z 1329.4 (intensity, 3.4×10^3) (fig. S4). Each of these ions showed the presence of iron based on the intensity of the ^{54}Fe isotope peak ($M^+ - 2$) compared to the major ^{56}Fe peak (M^+), resulting from the 5.8% natural abundance of ^{54}Fe. On the basis of isotopic compositions derived from the mass spectra, the majority of other observed ions in the MALDI-MS data likely derived from peptides bound to the amorphous carbon. Analysis of the m/z 932.3 compound suggested the presence of four irons based on the measured intensity of the ^{54}Fe peak, and an isotopic pattern indicating that carbon was the major other element present. This would suggest a molecular formula of Fe_4C_{58}. The detection of these compounds may provide a possible connection of iron with the production or function of the biogenic amorphous carbon.

Production of amorphous carbon by methanogenic archaea

To determine whether amorphous carbon production was unique to AOM consortia, the cell pellets of several different methanogens were analyzed. For *M. jannaschii*, *M. maripaludis*, and *M. barkeri*, the black color of the pellet was retained throughout each step in the procedure used for isolating amorphous carbon (Table 1). The black material was far less abundant in these methanogens compared with AOM cultures. Hence, it was difficult to purify and not possible to quantify the small amounts of carbon from the large amounts of biomass. Nonetheless, the presence of amorphous carbon in the final black samples from *M. jannaschii*, *M. maripaludis*, and *M. barkeri* was confirmed by Raman spectroscopy (Fig. 6, A and B) and XPS (Fig. 6, C and D, and fig. S5). Some cell pellets of other methanogens were black, but the black color vanished after washing with HCl (Table 1). In these cases, the black color of the original cell pellet was likely caused by FeS. Control experiments consisting of uninoculated media, filtered spent media, or inoculated cultures

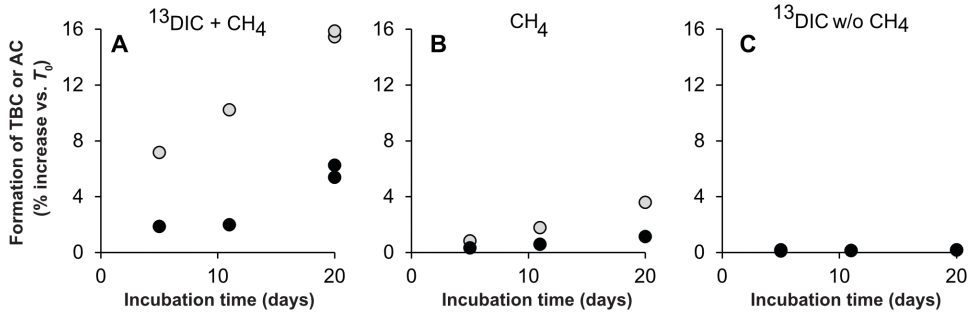

Fig. 5. Incorporation of inorganic carbon and methane into total biomass carbon (TBC) and amorphous carbon (AC). Assimilation of (**A**) DIC in the presence of methane, (**B**) methane, and (**C**) DIC in the absence of methane as energy source. Values are presented as fraction of carbon stock (in %) produced in the experiment. Gray circles present formation of TBC, and black circles present formation of AC. In (C), values for TBC are hidden behind similarly low values for AC.

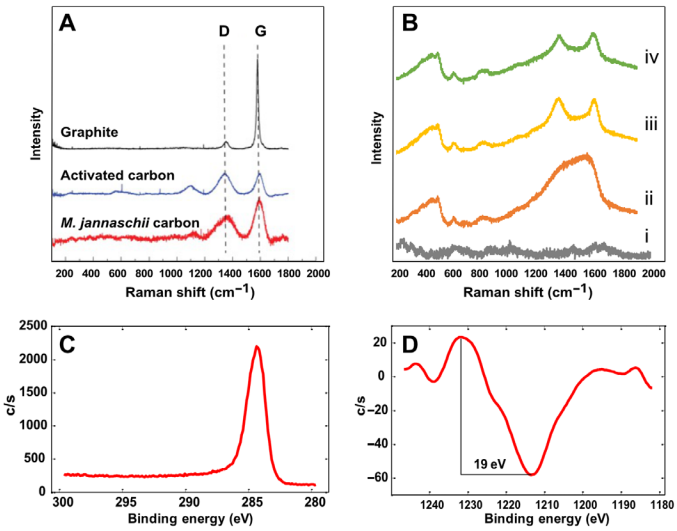

Fig. 6. Spectroscopic characterization of amorphous carbon from methanogens. (**A**) Raman spectrum of amorphous carbon isolated from *M. jannaschii* compared to select standards (activated carbon is Norit). Excitation was at 514 nm. (**B**) Raman spectra of white material from *E. coli* (spectrum i) compared to the spectra of black material containing amorphous carbon isolated from *M. maripaludis* grown on H_2/CO_2 (spectrum ii), *M. maripaludis* grown on formate (spectrum iii), and *M. barkeri* grown on acetate (spectrum iv). Excitation was at 514 nm. (**C**) The C1s XPS spectrum of an etched amorphous carbon sample from *M. maripaludis*, and (**D**) the corresponding C KLL spectrum indicating primarily sp^2 carbon bonds.

lacking H_2 (N_2/CO_2 provided without an electron donor) did not produce a carbonaceous pellet, thus indicating that the formation of amorphous carbon requires the presence of growing cells.

The Raman spectrum of the carbon isolated from *M. jannaschii* was compared with that observed for graphite and commercial activated carbon (Fig. 6A). The relative D/G peak intensity ratios indicate that the bulk of the carbon in the sample isolated from the methanogen is more similar to activated carbon (amorphous carbon) than graphite. This is also consistent with the Raman spectra of the carbon from other methanogens (Fig. 6B) and AOM consortia (Fig. 3). Raman analysis showed that *M. maripaludis* grown on both H_2/CO_2 and formate produced amorphous carbon (Fig. 6B, spectra ii and iii, respectively). On the basis of the size and color of the final black pellet from these cultures as well as the relative intensities of the Raman spectra, the amount of amorphous carbon was less in formate-grown cells compared with H_2/CO_2-grown cells. The two Raman spectra from different *M. maripaludis* cultures have unique features, indicating that the chemical nature of the carbon may be different and/or that the spectra are influenced by remaining biomolecules associated with the carbon. Last, the Raman spectrum of the black material from *M. barkeri* (Fig. 6B, spectrum iv) was similar to those from the other organisms studied here.

To test whether our extraction procedure caused formation of elemental carbon, a cell pellet of *Escherichia coli* was extracted. For *E. coli*, this extraction yielded a white residue that we assume is primarily cell wall material with some proteins. Raman spectra of several areas of that sample showed no characteristics of amorphous carbon (Fig. 6B, spectrum i). This shows that the carbon isolation procedure does not cause an abiotic production of amorphous carbon.

The isolated carbon samples from each methanogen were further characterized by XPS. Similar to the samples from AOM consortia, the surface of the carbon pellet was coated with proteins as indicated by the identification of nitrogen and oxygen (Table 2), as well as C═O bonds and C─N/C─O bonds observed in the C1s spectra (fig. S5). The etched samples were more carbon rich (Table 2) and contained primarily carbon-carbon bonds (Fig. 6C and fig. S5) that were sp^2 hybridized as evidenced by the D parameter of 19 eV in the C KLL spectrum (Fig. 6D and fig. S5). In summary, the XPS data show that the carbon isolated from the different methanogens has similar characteristics to the carbon isolated from AOM cultures.

An amorphous carbon sample from *M. maripaludis* grown on H_2/CO_2 had a $\delta^{13}C$ value of −31.8‰ (Table 3). This value is higher than those shown for ANME archaea that yields parts of the carbon from methane-derived DIC. Together, the presence of amorphous carbon in methanogens as well as AOM consortia supports its biochemical formation from conserved intermediates in the closely related pathways of methanogenesis and AOM.

DISCUSSION

Structure and origin of biogenic elemental carbon

Both AOM cultures and pure cultures of methanogens produce a black material that was identified as amorphous carbon. On the basis of the relative sizes and blackness of the pellets recovered from different cultures, ANME produce substantially more of this material compared with methanogens. The identity of the amorphous carbon was confirmed by Raman spectroscopy that showed the G and D bands characteristic of elemental carbon (Figs. 3D and 6,

A and B) (*44*, *45*). In graphite (black spectrum in Fig. 6A), the G band is intense and well resolved, while the D band is very low in intensity (in ideal graphite, the D band would be absent). In contrast, activated carbon, a form of amorphous carbon that lacks crystalline structure, has broad G and D bands of relatively equal intensities (Fig. 6A). For the black material isolated from the organisms studied here, the G and D bands are also broad with similar intensities, indicating a high level of disorder characteristic of amorphous carbon rather than crystalline graphite. The XPS data show that the carbon pellets are coated with residual proteins that contain sp^3 carbon; however, the bulk of the carbon below the surface is predominately sp^2 based on the D parameter of 19 eV in the C KLL spectra (Figs. 4D and 6D).

The amorphous carbon from ANME-1a/HotSeep-1 cultures was highly depleted in ^{13}C with $\delta^{13}C$ values of −60‰ (Table 3). The stable isotope probing experiments with $^{13}CH_4$ or ^{13}C-DIC showed that the amorphous carbon produced by ANME derived from DIC and methane-derived DIC (Fig. 5 and table S1). Thus, the isotope values of the carbon result from a combination of the original isotopic composition of DIC (−6‰), the provided methane (−41‰), and isotope fractionation during carbon fixation (*29*). Considering that in marine environments AOM results in $\delta^{13}C$-DIC values often down to −50 to −80‰ (*46*), amorphous carbon produced by ANME will have highly characteristic isotopic compositions, similar to those reported for ANME lipids (*17*, *40*, *47*). In the active AOM culture, the relative production or turnover of amorphous carbon is slower than the formation of the TBC. This suggests that the carbon accumulates in our cultivation procedure because of its highly inert nature. Thus, the presence of amorphous carbon with its characteristic isotope signatures might be an ideal marker to trace AOM activity in the geological record.

Summary of reactions that produce elemental carbon

To begin considering the processes that could potentially be associated with biochemically formed elemental carbon, we evaluated known reactions that form elemental carbon. In nature, carbon forms abiotically via one of three different routes:

1. $2CO \rightarrow C + CO_2$
2. $CO + H_2 \rightarrow C + H_2O$
3. $CO_2 \rightarrow C + O_2$

Reaction #1, the disproportionation of CO, is catalyzed by sulfide-oxide surfaces (*48*) and iron and silicon-iron single crystals (*49*). Reaction #2 represents the reduction of CO by hydrogen. Reaction #3 is known to proceed only when the oxygen produced is reduced by H_2, H_2S, Fe, Fe^{+2}, etc., to drive the reaction (*49*). All of these reactions occur at temperatures above 250°C, and one or more of them have been proposed for the generation of graphite crystals in hydrothermal vents (*50*).

Notably, methane-rich fluids have recently been shown to generate pure carbon in the form of diamond under very high pressure (5 to 7 GA) (*51*). This process occurs by the removal of hydrogen from methane:

4. $CH_4 \rightarrow C + 2H_2$

Another route for carbon formation comes from studies on soot formation, which propose that resonance-stabilized hydrocarbon-radical chain reactions are responsible for soot inception and growth (*52*, *53*). The first stage in this process is the production of ethylene or acetylene radicals that undergo radical chain reactions to generate polyaromatic hydrocarbons that then undergo further condensation reactions to form the final soot (carbon) particles (fig. S6) (*54*). This type of chemistry could be relevant in a biological system because the intermediate, ethylene, is a known biomolecule derived from *S*-adenosylmethionine (*55*), and radical biochemistry is abundant in anaerobes. However, abiotic soot formation reactions occur in flames at high combustion temperatures (1500 K). In addition, we did not observe any evidence of polycyclic aromatic hydrocarbons in samples from AOM consortia (see the Supplementary Materials). Furthermore, ethylene is an inhibitor of methanogenesis (*56*), further excluding this compound as a likely precursor to biogenic amorphous carbon.

The reactions producing amorphous carbon in ANME and methanogens are unclear, as they lack biological precedence. AOM and methanogenesis use the same central enzymes and coenzymes (fig. S1) (*22*, *57*), and our results indicate that the amorphous carbon produced in both ANME and methanogens is mostly derived from CO_2. Thus, the overall reaction could entail the reduction of carbon dioxide to generate pure carbon and water, which is thermodynamically favorable:

5. $CO_2 + 2H_2 \rightarrow C + 2H_2O\ \Delta G° = -79.8\ kJ\ mol^{-1}\ CO_2$

The catalytic machinery that would enable the production of elemental carbon is unknown and, thus, will be an important area for future work.

Potential physiological role(s) of amorphous carbon

The identification of amorphous carbon produced by methanogenic and methanotrophic archaea raises many questions surrounding its possible physiological functions. In both AOM consortia and in methanogens, the amorphous carbon may serve as a scaffolding material for the attachment and interaction with partner organisms or provide a protective barrier to increase resilience to toxic waste products. Alternatively, the carbon may facilitate the transfer of reducing equivalents between consortial partners. In sulfate-dependent AOM, the ANME oxidize methane to CO_2 and the partner bacteria perform sulfate reduction (*26*, *28*). Current evidence indicates that this interaction bases on direct interspecies electron transfer (DIET) (*23*, *24*). Similarly, some methanogens are also able to receive electrons from bacteria by DIET (*58*, *59*). The identification of intercellular wiring consisting of pili-like connecting structures has been reported as a mechanism for DIET in AOM consortia (*24*), and cytochrome-based electron transfer may also be involved (*60*, *61*). Considering the well-known electric conductivity of elemental carbon materials (*62*, *63*), the amorphous carbon may serve these archaea as a conductive element in interspecies electron transfer. This is supported by studies demonstrating that granular activated carbon promotes DIET between *M. barkeri* and *Geobacter metallireducens* (*64*).

The biogenic amorphous carbon identified here shares similarities in chemical composition and, possibly, in function to biochar, a carbon-rich material generated from thermochemical treatment (usually pyrolysis or gasification) of organic waste in oxygen-limited conditions (*65*). The elemental composition and chemical characteristics of biochar can vary widely depending on the type of biomass as well as the reaction conditions for its production. Although primarily carbonaceous, there are key functional groups present on the surface of biochar that result in its various useful properties. Like activated carbon, biochar has been shown to promote DIET through a proposed electron conduction role (*66*). Biochar is additionally proposed to enhance methanogenesis during

anaerobic digestion by serving as a pH buffer and acting as a surface for colonization (*67*). Other work has shown that biochar is redox active and can serve as an electron acceptor and an electron donor to drive microbial metabolism (*68*, *69*). Klupfel *et al.* (*69*) demonstrated that the ability of biochar to reversibly accept and donate electrons is due to the presence of quinone/quinol molecules. Most notably, biochar was recently demonstrated to serve as the sole electron acceptor for AOM by ANME-2d where the redox activity was attributed to its oxygen-based functional groups (*70*). Our XPS results showed that the surface of the black carbon pellets from the organisms studied here contained carbon bonded to heteroatoms including C─O/C─N and C═O/C─O─C. Some of these characteristics are due to adventitiously bound proteins, but similarly to biochar, the amorphous carbon could also be associated with or functionalized with redox active groups that act as electron sources/sinks or electron carriers.

Final remarks

The identification of biogenic amorphous carbon is a remarkable finding because elemental carbon formation was thought to occur only at elevated temperatures and pressures in chemical processes over geological time scales or as result of incomplete burning of organic materials. Difficulties associated with completely purifying and accurately quantifying the amorphous carbon currently preclude more detailed investigations of its function and biosynthesis. Thus, future studies will be required to determine the metabolic origin and function of amorphous carbon in the context of complex microbial consortia. Because of the wide distribution and abundance of ANME and methanogens, the biogenic formation of amorphous carbon may have important roles in carbon cycling and climate regulation. This carbon may persist in sediments over geological time scales and thus may represent a so far overlooked carbon sink in nature.

MATERIALS AND METHODS

Chemicals

Powdered pyrite (FeS_2) was obtained by grinding a natural sample of pyrite in mortar and pestle to a fine powder. Because both natural as well as synthetic pyrites are generally not stoichiometrically pure (*71*), we used natural pyrite for our reference sample. Trolite (FeS) was chemically prepared by mixing aqueous anoxic solutions of $FeCl_2$ and Na_2S to produce a black FeS precipitate. All other compounds and reagents were obtained from Sigma-Aldrich, now MilliporeSigma.

Origin and cultivation of AOM enrichments

The thermophilic AOM50 consortia were cultured from hydrothermal vent sediments collected from mat-covered sites in the Guaymas Basin, Gulf of California, Mexico (27.7438°N, 111.4091°W) during the RV Atlantis cruise AT15-56 in November/December 2009 (Alvin Dive 4570) (*27*). The AOM20 consortia (ANME-2a/2c and SeepSRB1/SeepSRB2 dominated cultures) derives form AMON Mud Volcano Eastern Mediterranean Sea (31.71°N, 32.37°E) sampled during the NAUTINIL expedition with RV L'Atalante in September 2003 (*28*, *29*).

Sediments from both sites were incubated with sulfate reducer medium prepared after Widdel and Bak (*72*) and with a headspace composition of CH_4 and CO_2 as outlined (*73*). Methane [0.225 MPa CH_4 (gas)] and sulfate [28 mM SO_4^{2-} (aq)] were provided as the sole electron donor and acceptor, respectively, and carbon dioxide (0.025 MPa CO_2; 30 mM DIC) as the carbon source. Cultivation was performed at 50°C for the AOM50 culture, and room temperature (20°C) for the AOM20 culture. Culture media were exchanged when sulfide concentrations exceeded ~12 mM, and samples were regularly diluted (1:2; 1:4). Both cultures were sediment free after 2 to 3 years. The extensive exchange and dilution of cultures would have eliminated any elemental carbon that may have been in the original sediment sample. To determine the molecular inventory of the cultures, 450 ml of culture was harvested at about 10 mM sulfide content. Under anoxic conditions, cells were centrifuged, and cell pellets were immediately frozen. The cell pellets and the spent media were sent from Germany to the United States on dry ice.

Incorporation of ^{13}C-DIC and $^{13}CH_4$ into amorphous carbon by active AOM50 cultures

To establish whether methane or CO_2/DIC was the primary source of the amorphous carbon produced by AOM consortia and to determine the effect of methane supply on DIC assimilation, 600 ml of AOM50 culture was pooled and equally distributed into ten 150-ml culture bottles with 100 ml of medium. These cultures were incubated either with 5% ^{13}C-DIC supplied with or without methane headspace (2 atm) or with 5% $^{13}CH_4$ in 2 atm CH_4. These cultures were incubated at 50°C on a shaking table and sampled for carbon measurements (see below). The DIC background was 30 mM. At the beginning and the end, each experiment was sampled for DIC (2 ml of sterile filtered medium into 2-ml vials) and methane (1 ml of gas phase into 12-ml Exetainer filled with 1 ml of NaOH). To measure DIC isotopic compositions, 100 µl of phosphoric acid (45%) was added to 12-ml Exetainer vials, the headspace was replaced with synthetic air, and 0.5 ml of filtered medium was injected through the septum. After 10 hours of equilibration, the CO_2 isotopic composition was measured by isotope ratio infrared spectroscopy (Thermo Fisher Scientific Delta Ray Isotope Ratio Infrared Spectrometer with Universal Reference Interface Connect and Cetac ASX-7100 Autosampler). The ^{13}C-DIC measurements were calibrated with a reference gas against Vienna Pee Dee belemnite (VPDB). To measure methane carbon isotopic compositions, 200 µl of gas phase of the Exetainer was injected into a Thermo Finnigan Trace GC coupled via a combustion interface III to a Thermo Finnigan Delta plus XP isotope ratio mass spectrometer. The gas chromatography used on a Carboxen-1006 PLOT fused-silica capillary column (length, 30 m; internal diameter, 0.32 mm; isothermal column temperature, 40°C). The $\delta^{13}C$ measurements were calibrated with CO_2 reference gas of known isotopic composition. At the end of the experiment, the particulate matter of each sample was collected by centrifugation. Inorganic carbon was removed by three times washing with HCl (0.1 mM). Two subsamples (1/20 of the samples) were taken for the determination of TBC and washed twice with water and methanol and transferred into tin cups (5 mm by 9 mm; HEKAtech) and dried. The residual samples were treated three times with 1 M NaOH and heated for 10 min to 100°C. After that, samples were washed and heated three times with 1 M HCl, twice with water, transferred with methanol into tin cups, and dried to analyze the isotopic composition of the purified amorphous carbon. Carbon stable isotopic compositions of the samples were measured with a Thermo Finnigan Flash EA 2000 elemental analyzer connected to a Delta V Plus isotope ratio mass spectrometer (IRMS). The combustion temperature was 999°C; the carrier gases and oxidation reagents were He (100 ml^{-1}) and O_2 (200 ml min^{-1}). The chromatographic separation was performed with an IRMS steel separation column (length, 300 cm;

outer diameter, 6 mm; internal diameter, 5 mm; kept at 40°C). All carbon isotope values were converted into isotope fractions. The relative substrate-specific (DIC, CH_4) rates of carbon formation (C_+; as % of the carbon stock) was calculated according to

$$\%C_+(\%) = \frac{fC_t - fC_o}{fS_m - fS_0} \times 100$$

with the fractions (f) of the measured carbon product (total carbon or amorphous carbon) at the start (0) or end (t) of the experiment and the average fractions of the labeled substrate DIC or CH_4 (S_m) compared to the nonlabeled conditions (S_0).

Source and cultivation of methanogens

M. maripaludis S2 902 (original cultures supplied by J. A. Leigh, University of Washington) was grown in McN medium (*74*) with H_2/CO_2 at 275 kPa or in formate medium (*75*). *Methanosarcina acetivorans* (original cultures supplied by J. Gregory Ferry, Penn State University) was grown in high-salt (0.4 M NaCl) medium (*76*) with methanol (125 mM). *M. jannaschii* was grown as described (*77*) and obtained from K. R. Sowers (University of Maryland Baltimore County) as a frozen cell pellet. Cell pellets of *Methanococcus vannielii* were obtained from R. Wolfe and stored at −80°C. Acetate grown *M. barkeri* cells were supplied by D. Grahame and stored at −80°C. The other organisms described in Table 1 were supplied by S. Shima (Max Planck Institute for Terrestrial Microbiology, Marburg, Germany), grown as previously reported (*78*), and stored as frozen cell pellets at −80°C.

Procedure for extraction and analysis of black material containing amorphous carbon

The moist cell pellets (10 to 30 mg) were washed with water and then with 2 ml of 1 M NaOH to remove cellular proteins. This was repeated three times with 1-min heating at 100°C. The resulting black pellet was then treated with 1 M HCl for 5 min at 100°C to remove insoluble iron-containing minerals in the sample. Treatment of chemical standards of FeS_2 or FeS revealed that FeS_2 was not removed in this process but FeS was removed. Both of these compounds were tested because both could produce a black color in the sample. For samples that still had black particles remaining after the 1 M HCl treatment, they were processed and analyzed further for the presence of elemental carbon. Thus, the black pellet was washed three times with water to remove salts, then with methanol, followed by drying at 100°C. Last, portions of the resulting black pellets were assayed by Raman spectroscopy to establish the presence of elemental carbon, XPS to determine elemental composition, and for $\delta^{13}C$ abundance by MS of the carbon dioxide after combustion with oxygen. In other experiments, the resulting black pellet from HCl treatment was then subjected to 70% and/or 100% nitric acid at 100°C. The 70% nitric acid treatment removed the remaining FeS_2, and prolonged (~2 days) treatment with 100% nitric acid at 100°C could solubilize the amorphous carbon.

Alternate extraction procedure for *M. maripaludis* and *E. coli*

For *M. maripaludis* grown on either hydrogen or formate, cell pellets (wet weight, ~1 g) were extracted two times with methanol to remove lipids and media salts. The resulting pellets were split into two identical samples. One of each of these samples was dried for 24 hours at ~60°C in air for direct analysis by Raman spectroscopy. The other sample was then extracted with 1 M NaOH and 1 M HCl as described above. After a water wash, the samples were dried for 24 hours at ~60°C in air for Raman analysis. This procedure was also carried out with an *E. coli* cell pellet (grown in Luria-Bertani broth) as a negative control. The final *E. coli* sample after NaOH and HCl treatments consisted of a white pellet, which we assume is mostly cell wall material. Conversely, the final samples from *M. maripaludis* contained a black material that was a larger amount in hydrogen-grown cells compared with formate-grown cells. This black material along with the white pellet from *E. coli* were analyzed by Raman spectroscopy (data shown in Fig. 6B). For the methanol-extracted *M. maripaludis* cells without additional NaOH and HCl treatments, we could not confirm the presence of amorphous carbon directly by Raman because of the abundance of other biomolecules that interfere with the detection.

Quantitative analysis of amorphous carbon recovered from ANME-2a/c/Seep-SRB cell pellets

A 79-mg portion of the black wet ANME-2a/c/Seep-SRB cell pellet was dried to produce 15.8 mg of a dark gray solid, indicating that the pellet was 80% water. Extraction of this solid with 500 µl of 1.0 M NaOH for 5 min at 100°C released ~0.4 mg of protein as determined by a Bradford assay. The presence of proteins in this extract was also confirmed by SDS-PAGE analysis. On the basis of established data showing that ~55% of the dried weight of *E. coli* is protein (*79*), one can calculate that only ~5% of the dried pellet was from cells. After an additional extraction with 500 µl of 1.0 M NaOH for 5 min at 100°C, the resulting black solid isolated by centrifugation was extracted two times with 500 µl of 1.0 M HCl for 5 min at 100°C to solubilize and remove abundant minerals, followed by a wash with deionized water to remove any remaining salts. The resulting black pellet was then extracted overnight at room temperature with 100 µl of 0.1 M EDTA (pH ~4.0) to further remove any metals not removed by preceding steps. After the removal of the EDTA solution by centrifugation, the pellet was washed three times with water and then extracted with methanol to remove any lipids. This final dried pellet weight was ~0.5 mg, showing that the original dried biomass (15.8 mg) contained ~3.2% amorphous carbon by weight.

Raman spectroscopy

Raman spectra were collected on the partially purified elemental carbon samples (purification process described above) using a JY Horiba LabRam HR (800 mm spectrometer) Raman microprobe using a slit width of 150 µm, confocal aperture of 400 µm, 600 grooves/mm grating, and a 100× microscope objective (numerical aperture, 0.90). Excitation was provided by a 514-nm (green) Laser Physics 100S-514 Ar^+ laser. The D (disorder/defect) and G (graphite) peaks of carbon located nominally at ~1360 and ~1560 cm^{-1}, respectively (*32*), were of interest to this study, and thus, the spectral range of 100 to 1800 cm^{-1} was measured for each sample to detect the presence of carbonaceous material. Extended spectral ranges (100 to 4000 cm^{-1}) were also collected for some samples to check for the presence of an additional band located at ~2900 cm^{-1} that is not often found in unstructured carbon (*44*). Interactions between the carbonaceous material and the laser beam may result in damage to the sample and lead to incorrect interpretations concerning the nature of the carbon-bearing material (*45*, *80*, *81*). Thus, shorter collection times and lower laser power at the sample are often used (*82*). Here, measurements were collected for 10 to 30 s over three accumulations because using a longer collection time was found to damage the

sample. Laser power was also reduced to 10% of the total output power at the sample. Spectra from damage-induced measurements are not presented here as the interaction between the laser and the carbonaceous material that causes the damage both weakens the signal and changes the intensity and width of the D band. Spectra were analyzed using the LabSpec 5 software suite. This method was also used for the analysis of additional compounds present the samples, identification of which was accomplished using the CrystalSleuth software and database.

XPS analysis

XPS characterization of the samples was performed on a PHI VersaProbe III scanning XPS microscope using monochromatic Al K-alpha x-ray source (1486.6 eV). XPS spectra were acquired with various beam settings (50/100/200 μm) commensurate with sample sizes and dual beam charge neutralization. All binding energies were referenced to C—C peak at 284.8 eV. Atomic concentration % of elements was determined from the integrated intensity of the elemental photoemission features corrected by relative atomic sensitivity factors.

Measurement of natural isotopic composition of amorphous carbon from ANME and *M. maripaludis*

A weighed portion (0.1 to 0.25 mg) of the isolated amorphous carbon was placed in a tin capsule (9 mm by 5 mm). Stable carbon isotope analyses were performed using an Elementar vario ISOTOPE cube elemental analyzer that combust the carbon to CO_2 coupled to an Isoprime 100 continuous flow isotope ratio mass spectrometer that measures the abundances of the masses of the produced CO_2 (44 to 46). The measurements were calibrated to VPDB using three-point linear normalization (IAEA CH6, IAEA CH7, Elemental Microanalysis with wheat flour).

MALDI-MS analysis of amorphous carbon

MALDI mass spectral analysis of the partially purified elemental carbon pellet was performed using an AB Sciex 4800 MALDI TOF/TOF operated in reflector positive ion mode using α-cyanohydroxycinnamic acid as a matrix. Samples were scanned from 799 to 4013 *m*/*z*.

SUPPLEMENTARY MATERIALS

Supplementary material for this article is available at https://science.org/doi/10.1126/sciadv.abg9739

View/request a protocol for this paper from *Bio-protocol*.

REFERENCES AND NOTES

1. D. D. L. Chung, Review graphite. *J. Mater. Sci.* **37**, 1475–1489 (2002).
2. A. Petzold, J. A. Ogren, M. Fiebig, P. Laj, S. M. Li, U. Baltensperger, T. Holzer-Popp, S. Kinne, G. Pappalardo, N. Sugimoto, C. Wehrli, A. Wiedensohler, X. Y. Zhang, Recommendations for reporting "black carbon" measurements. *Atmos. Chem. Phys.* **13**, 8365–8379 (2013).
3. N. L. Briggs, C. M. Long, Critical review of black carbon and elemental carbon source apportionment in Europe and the United States. *Atmos. Environ.* **144**, 409–427 (2016).
4. Q. H. S. Chan, M. E. Zolensky, R. J. Bodnar, C. Farley, J. C. H. Cheung, Investigation of organo-carbonate associations in carbonaceous chondrites by Raman spectroscopy. *Geochim. Cosmochim. Acta* **201**, 392–409 (2017).
5. N. Singh, S. Abiven, M. S. Torn, M. W. I. Schmidt, Fire-derived organic carbon in soil turns over on a centennial scale. *Biogeosciences* **9**, 2847–2857 (2012).
6. S. Bruun, E. S. Jensen, L. S. Jensen, Microbial mineralization and assimilation of black carbon: Dependency on degree of thermal alteration. *Org. Geochem.* **39**, 839–845 (2008).
7. M. C. Potter, Bacteria as agents in the oxidation of amorphous carbon. *Proc. R. Soc. Lond. B-Conta* **80**, 239–259 (1908).
8. Y. Kuzyakov, I. Subbotina, H. Q. Chen, I. Bogomolova, X. L. Xu, Black carbon decomposition and incorporation into soil microbial biomass estimated by ^{14}C labeling. *Soil Biol. Biochem.* **41**, 210–219 (2009).
9. A. R. Zimmerman, Abiotic and microbial oxidation of laboratory-produced black carbon (biochar). *Environ. Sci. Technol.* **44**, 1295–1301 (2010).
10. M. Szczesna-Antczak, A. Kaczorowska, W. Kaczorowski, T. Antczak, Biomodification and biodeterioration of carbon coatings by fungal strains. *Int. Biodeter. Biodegr.* **88**, 106–117 (2014).
11. L. M. Sekhohola, M. L. Isaacs, A. K. Cowan, Fungal colonization and enzyme-mediated metabolism of waste coal by Neosartorya fischeri strain ECCN 84. *Biosci. Biotechnol. Biochem.* **78**, 1797–1802 (2014).
12. Z. Lyu, N. Shao, T. Akinyemi, W. B. Whitman, Methanogenesis. *Curr. Biol.* **28**, R727–R732 (2018).
13. S. Kirschke, P. Bousquet, P. Ciais, M. Saunois, J. G. Canadell, E. J. Dlugokencky, P. Bergamaschi, D. Bergmann, D. R. Blake, L. Bruhwiler, P. Cameron-Smith, S. Castaldi, F. Chevallier, L. Feng, A. Fraser, M. Heimann, E. L. Hodson, S. Houweling, B. Josse, P. J. Fraser, P. B. Krummel, J. F. Lamarque, R. L. Langenfelds, C. le Quéré, V. Naik, S. O'Doherty, P. I. Palmer, I. Pison, D. Plummer, B. Poulter, R. G. Prinn, M. Rigby, B. Ringeval, M. Santini, M. Schmidt, D. T. Shindell, I. J. Simpson, R. Spahni, L. P. Steele, S. A. Strode, K. Sudo, S. Szopa, G. R. van der Werf, A. Voulgarakis, M. van Weele, R. F. Weiss, J. E. Williams, G. Zeng, Three decades of global methane sources and sinks. *Nat. Geosci.* **6**, 813–823 (2013).
14. S. J. Hallam, N. Putnam, C. M. Preston, J. C. Detter, D. Rokhsar, P. M. Richardson, E. DeLong, Reverse methanogenesis: Testing the hypothesis with environmental genomics. *Science* **305**, 1457–1462 (2004).
15. S. Bhattarai, C. Cassarini, P. N. L. Lens, Physiology and distribution of archaeal methanotrophs that couple anaerobic oxidation of methane with sulfate reduction. *Microbiol. Mol. Biol. Rev.* **83**, 10.1128/MMBR.00074-18, (2019).
16. W. S. Reeburgh, Oceanic methane biogeochemistry. *Chem. Rev.* **107**, 486–513 (2007).
17. K. U. Hinrichs, J. M. Hayes, S. P. Sylva, P. G. Brewer, E. F. DeLong, Methane-consuming archaebacteria in marine sediments. *Nature* **398**, 802–805 (1999).
18. V. J. Orphan, K. U. Hinrichs, W. Ussler III, C. K. Paull, L. T. Taylor, S. P. Sylva, J. M. Hayes, E. F. Delong, Comparative analysis of methane-oxidizing archaea and sulfate-reducing bacteria in anoxic marine sediments. *Appl. Environ. Microbiol.* **67**, 1922–1934 (2001).
19. A. A. Raghoebarsing, A. Pol, K. T. van de Pas-Schoonen, A. J. P. Smolders, K. F. Ettwig, W. I. C. Rijpstra, S. Schouten, J. S. S. Damsté, H. J. M. op den Camp, M. S. M. Jetten, M. Strous, A microbial consortium couples anaerobic methane oxidation to denitrification. *Nature* **440**, 918–921 (2006).
20. M. F. Haroon, S. Hu, Y. Shi, M. Imelfort, J. Keller, P. Hugenholtz, Z. Yuan, G. W. Tyson, Anaerobic oxidation of methane coupled to nitrate reduction in a novel archaeal lineage. *Nature* **500**, 567–570 (2013).
21. K. Knittel, T. Losekann, A. Boetius, R. Kort, R. Amann, Diversity and distribution of methanotrophic archaea at cold seeps. *Appl. Environ. Microbiol.* **71**, 467–479 (2005).
22. P. H. Timmers, C. U. Welte, J. J. Koehorst, C. M. Plugge, M. S. M. Jetten, A. J. M. Stams, Reverse methanogenesis and respiration in methanotrophic archaea. *Archaea* **2017**, 1654237 (2017).
23. S. E. McGlynn, G. L. Chadwick, C. P. Kempes, V. J. Orphan, Single cell activity reveals direct electron transfer in methanotrophic consortia. *Nature* **526**, 531–535 (2015).
24. G. Wegener, V. Krukenberg, D. Riedel, H. E. Tegetmeyer, A. Boetius, Intercellular wiring enables electron transfer between methanotrophic archaea and bacteria. *Nature* **526**, 587–590 (2015).
25. V. Krukenberg, D. Riedel, H. R. Gruber-Vodicka, P. L. Buttigieg, H. E. Tegetmeyer, A. Boetius, G. Wegener, Gene expression and ultrastructure of meso- and thermophilic methanotrophic consortia. *Environ. Microbiol.* **20**, 1651–1666 (2018).
26. A. Boetius, K. Ravenschlag, C. J. Schubert, D. Rickert, F. Widdel, A. Gieseke, R. Amann, B. B. Jørgensen, U. Witte, O. Pfannkuche, A marine microbial consortium apparently mediating anaerobic oxidation of methane. *Nature* **407**, 623–626 (2000).
27. T. Holler, F. Widdel, K. Knittel, R. Amann, M. Y. Kellermann, K. U. Hinrichs, A. Teske, A. Boetius, G. Wegener, Thermophilic anaerobic oxidation of methane by marine microbial consortia. *ISME J.* **5**, 1946–1956 (2011).
28. G. Wegener, V. Krukenberg, S. E. Ruff, M. Y. Kellermann, K. Knittel, Metabolic capabilities of microorganisms involved in and associated with the anaerobic oxidation of methane. *Front. Microbiol.* **7**, (2016).
29. T. Holler, G. Wegener, K. Knittel, A. Boetius, B. Brunner, M. M. M. Kuypers, F. Widdel, Substantial (13) C/(12) C and D/H fractionation during anaerobic oxidation of methane by marine consortia enriched in vitro. *Environ. Microbiol. Rep.* **1**, 370–376 (2009).
30. V. Krukenberg, K. Harding, M. Richter, F. O. Glöckner, H. R. Gruber-Vodicka, B. Adam, J. S. Berg, K. Knittel, H. E. Tegetmeyer, A. Boetius, G. Wegener, Candidatus Desulfofervidus auxilii, a hydrogenotrophic sulfate-reducing bacterium involved in the thermophilic anaerobic oxidation of methane. *Environ. Microbiol.* **18**, 3073–3091 (2016).

31. R. Burgess, C. Buono, P. R. Davies, R. J. Davies, T. Legge, A. Lai, R. Lewis, D. J. Morgan, N. Robinson, D. J. Willock, The functionalisation of graphite surfaces with nitric acid: Identification of functional groups and their effects on gold deposition. *J. Catal.* **323**, 10–18 (2015).
32. A. C. Ferrari, Raman spectroscopy of graphene and graphite: Disorder, electron-phonon coupling, doping and nonadiabatic effects. *Solid State Commun.* **143**, 47–57 (2007).
33. A. Merlen, J. G. Buijnsters, C. Pardanaud, A guide to and review of the use of multiwavelength raman spectroscopy for characterizing defective aromatic carbon solids: From graphene to amorphous carbons. *Coatings* **7**, 153 (2017).
34. A. C. Ferrari, J. Robertson, Interpretation of Raman spectra of disordered and amorphous carbon. *Phys. Rev. B* **61**, 14095–14107 (2000).
35. W. J. B. Dufresne, C. J. Rufledt, C. P. Marshall, Raman spectroscopy of the eight natural carbonate minerals of calcite structure. *J. Raman Spectrosc.* **49**, 1999–2007 (2018).
36. J. Diaz, G. Paolicelli, S. Ferrer, F. Comin, Separation of the sp3and sp2 components in the C1s photoemission spectra of amorphous carbon films. *Phys Rev B* **54**, 8064–8069 (1996).
37. A. Mezzi, S. Kaciulis, Surface investigation of carbon films: From diamond to graphite. *Surf. Interface Anal.* **42**, 1082–1084 (2010).
38. H. Torabizadeh, All proteins have a basic molecular formula. *World Acad. Sci. Eng. Technol.* **78**, 961–965 (2011).
39. V. J. Orphan, C. H. House, K. U. Hinrichs, K. D. McKeegan, E. F. DeLong, Methane-consuming archaea revealed by directly coupled isotopic and phylogenetic analysis. *Science* **293**, 484–487 (2001).
40. M. Y. Kellermann, G. Wegener, M. Elvert, M. Y. Yoshinaga, Y. S. Lin, T. Holler, X. P. Mollar, K. Knittel, K. U. Hinrichs, Autotrophy as a predominant mode of carbon fixation in anaerobic methane-oxidizing microbial communities. *Proc. Natl. Acad. Sci. U.S.A.* **109**, 19321–19326 (2012).
41. T. Treude, V. Orphan, K. Knittel, A. Gieseke, C. H. House, A. Boetius, Consumption of methane and CO2 by methanotrophic microbial mats from gas seeps of the anoxic Black Sea. *Appl. Environ. Microbiol.* **73**, 2271–2283 (2007).
42. M. V. Kharlamova, V. N. Mochalin, M. R. Lukatskaya, J. Niu, V. Presser, S. Mikhalovsky, Y. Gogotsi, Adsorption of proteins in channels of carbon nanotubes: Effect of surface chemistry. *Mater. Express* **3**, 1–10 (2013).
43. S. Ray, A. G. Shard, Quantitative analysis of adsorbed proteins by x-ray photoelectron spectroscopy. *Anal. Chem.* **83**, 8659–8666 (2011).
44. A. Cuesta, P. Dhamelincourt, J. Laureyns, A. Martinezalonso, J. M. D. Tascon, Raman microprobe studies on carbon materials. *Carbon* **32**, 1523–1532 (1994).
45. N. K. Lunsdorf, I. Dunkl, B. C. Schmidt, G. Rantitsch, H. von Eynatten, Towards a higher comparability of geothermometric data obtained by raman spectroscopy of carbonaceous material. Part I: Evaluation of biasing factors. *Geostand. Geoanal. Res.* **38**, 73–94 (2014).
46. M. J. Whiticar, Carbon and hydrogen isotope systematics of bacterial formation and oxidation of methane. *Chem. Geol.* **161**, 291–314 (1999).
47. H. Niemann, M. Elvert, Diagnostic lipid biomarker and stable carbon isotope signatures of microbial communities mediating the anaerobic oxidation of methane with sulphate. *Org. Geochem.* **39**, 1668–1677 (2008).
48. E. A. Mathez, J. R. Delaney, The nature and distribution of carbon in submarine basalts and peridotite nodules. *Earth Planet. Sci. Lett.* **56**, 217–232 (1981).
49. G. D. Renshaw, C. Roscoe, P. L. Walker, Disproportionation of CO: 1. Over iron and silicon-iron single crystals. *J. Catal.* **18**, 164–183 (1970).
50. J. Jedwab, J. Boulegue, Graphite crystals in hydrothermal vents. *Nature* **310**, 41–43 (1984).
51. V. Matjuschkin, A. B. Woodland, D. J. Frost, G. M. Yaxley, Reduced methane-bearing fluids as a source for diamond. *Sci. Rep.* **10**, 6961 (2020).
52. K. O. Johansson, M. P. Head-Gordon, P. E. Schrader, K. R. Wilson, H. A. Michelsen, Resonance-stabilized hydrocarbon-radical chain reactions may explain soot inception and growth. *Science* **361**, 997–1000 (2018).
53. M. Frenklach, Reaction mechanism of soot formation in flames. *Phys. Chem. Chem. Phys.* **4**, 2028–2037 (2002).
54. H. Wang, Formation of nascent soot and other condensed-phase materials in flames. *Proc. Combust Inst.* **33**, 41–67 (2011).
55. D. O. Adams, S. F. Yang, 1-aminocyclopropane-1-carboxylate synthase. *Methods Enzymol.* **143**, 426–429 (1987).
56. B. Schink, Inhibition of methanogenesis by ethylene and other unsaturated-hydrocarbons. *FEMS Microbiol. Ecol.* **31**, 63–68 (1985).
57. R. K. Thauer, Biochemistry of methanogenesis: A tribute to Marjory Stephenson. 1998 Marjory Stephenson Prize Lecture. *Microbiology* **144** (Pt 9), 2377–2406 (1998).
58. A. E. Rotaru, P. M. Shrestha, F. Liu, B. Markovaite, S. Chen, K. P. Nevin, D. R. Lovley, Direct interspecies electron transfer between Geobacter metallireducens and Methanosarcina barkeri. *Appl. Environ. Microbiol.* **80**, 4599–4605 (2014).
59. A. E. Rotaru, P. M. Shrestha, F. Liu, M. Shrestha, D. Shrestha, M. Embree, K. Zengler, C. Wardman, K. P. Nevin, D. R. Lovley, A new model for electron flow during anaerobic digestion: Direct interspecies electron transfer to Methanosaeta for the reduction of carbon dioxide to methane. *Energ. Environ. Sci.* **7**, 408–415 (2014).
60. S. Scheller, H. Yu, G. L. Chadwick, S. E. McGlynn, V. J. Orphan, Artificial electron acceptors decouple archaeal methane oxidation from sulfate reduction. *Science* **351**, 703–707 (2016).
61. C. T. Skennerton, K. Chourey, R. Iyer, R. L. Hettich, G. W. Tyson, V. J. Orphan, Erratum for Skennerton et al., "methane-fueled syntrophy through extracellular electron transfer: Uncovering the genomic traits conserved within diverse bacterial partners of anaerobic methanotrophic archaea". *MBio* **8**, 10.1128/mBio.01561-17, (2017).
62. D. D. L. Chung, Electrical applications of carbon materials. *J. Mater. Sci.* **39**, 2645–2661 (2004).
63. L. Kavan, Electrochemical carbon. *Chem. Rev.* **97**, 3061–3082 (1997).
64. F. H. Liu, A.-E. Rotaru, P. M. Shrestha, N. S. Malvankar, K. P. Nevin, D. R. Lovley, Promoting direct interspecies electron transfer with activated carbon. *Energ. Environ. Sci.* **5**, 8982–8989 (2012).
65. P. R. Yaashikaa, P. S. Kumar, S. Varjani, A. Saravanan, A critical review on the biochar production techniques, characterization, stability and applications for circular bioeconomy. *Biotechnol. Rep. (Amst.)* **28**, e00570 (2020).
66. S. Chen, A.-E. Rotaru, P. M. Shrestha, N. S. Malvankar, F. Liu, W. Fan, K. P. Nevin, D. R. Lovley, Promoting interspecies electron transfer with biochar. *Sci. Rep.* **4**, 5019 (2014).
67. J. Ma, J. Pan, L. Qiu, Q. Wang, Z. Zhang, Biochar triggering multipath methanogenesis and subdued propionic acid accumulation during semi-continuous anaerobic digestion. *Bioresour. Technol.* **293**, 122026 (2019).
68. J. M. Saquing, Y. H. Yu, P. C. Chiu, Wood-derived black carbon (biochar) as a microbial electron donor and acceptor. *Environ. Sci. Technol. Lett.* **3**, 62–66 (2016).
69. L. Klupfel, M. Keiluweit, M. Kleber, M. Sander, Redox properties of plant biomass-derived black carbon (biochar). *Environ. Sci. Technol.* **48**, 5601–5611 (2014).
70. X. Q. Zhang, J. Xia, J. Pu, C. Cai, G. W. Tyson, Z. Yuan, S. Hu, Biochar-mediated anaerobic oxidation of methane. *Environ. Sci. Technol.* **53**, 6660–6668 (2019).
71. S. Kar, S. K. Mandal, D. Das, S. Chaudhuri, Wet chemical synthesis of iron pyrite and characterization by Mössbauer spectroscopy. *Mater. Lett.* **58**, 2886–2889 (2004).
72. F. B. Widdel, *The Prokaryotes*, D. M. Trüper, W. Harder, K.-H. Schleifer, Eds. (Springer, New York, ed. 2, 2002).
73. R. Laso-Perez, V. Krukenberg, F. Musat, G. Wegener, Establishing anaerobic hydrocarbon-degrading enrichment cultures of microorganisms under strictly anoxic conditions. *Nat. Protoc.* **13**, 1310–1330 (2018).
74. F. Sarmiento, J. A. Leigh, W. B. Whitman, Genetic systems for hydrogenotrophic methanogens. *Methods Enzymol.* **494**, 43–73 (2011).
75. F. Long, L. L. Wang, B. Lupa, W. B. Whitman, A flexible system for cultivation of *methanococcus* and other formate-utilizing methanogens. *Archaea* **2017**, 1–12 (2017).
76. K. R. Sowers, J. E. Boone, R. P. Gunsalus, Disaggregation of methanosarcina spp. and growth as single cells at elevated osmolarity. *Appl. Environ. Microbiol.* **59**, 3832–3839 (1993).
77. B. Mukhopadhyay, E. F. Johnson, R. S. Wolfe, Reactor-scale cultivation of the hyperthermophilic methanarchaeon *Methanococcus jannaschii* to high cell densities. *Appl. Environ. Microbiol.* **65**, 5059–5065 (1999).
78. R. H. White, Identification and biosynthesis of 1-mercaptoethanesulfonic acid (1-MES), an analogue of coenzyme M, found widely in the methanogenic archaea. *Biochemistry* **56**, 6137–6144 (2017).
79. F. C. Neidhardt, H. E. Umbarger, Chemical Composition of Escherichia coli in, *Escherichia coli and Salmonella Cellular and Molecular Biology*, F. C. Neidhardt, Ed. (ASM Press, Washington D.C., ed. 2, 1996), vol. 1.
80. A. C. Allwood, M. R. Walter, C. P. Marshall, Raman spectroscopy reveals thermal palaeoenvironments of c.3.5 billion-year-old organic matter. *Vib. Spectrosc.* **41**, 190–197 (2006).
81. D. G. Henry, I. Jarvis, G. Gillmore, M. Stephenson, J. F. Emmings, Assessing low-maturity organic matter in shales using Raman spectroscopy: Effects of sample preparation and operating procedure. *Int. J. Coal Geol.* **191**, 135–151 (2018).
82. O. Beyssac, B. Goffé, J. P. Petitet, E. Froigneux, M. Moreau, J. N. Rouzaud, On the characterization of disordered and heterogeneous carbonaceous materials by Raman spectroscopy. *Spectrochim. Acta A* **59**, 2267–2276 (2003).
83. G. M. Gadd, Metals, minerals and microbes: Geomicrobiology and bioremessdiation. *Microbiol. Sgm.* **156**, 609–643 (2010).

Acknowledgments: We thank W. Keith Ray (Virginia Tech) for the mass spectroscopy analyses, R. Reid (Virginia Tech) for obtaining the carbon isotope measurements in Table 3, and D. Slade (Virginia Tech) and B. Geier (MPI Bremen) for obtaining light microscope images. **Funding:** This work was supported by the National Science Foundation grant MCB1120346 (R.H.W.). G.W. was supported by the DFG excellence cluster 2077 "The Ocean Floor - Earth's Uncharted Interface" at MARUM, University of Bremen and the Max Planck Society. Partial funding for R.J.B.'s research activities is provided by the National Science Foundation under grant EAR-1624589. SEM/EDS and XPS analyses were performed at the Surface Analysis Laboratory in the Department of Chemistry at Virginia Tech, which is supported by the National Science Foundation under grant no. CHE-1531834. The mass spectrometry resources are maintained by the Virginia Tech Mass Spectrometry Incubator, a facility operated, in part, through funding

by the Fralin Life Science Institute at Virginia Tech and by the Agricultural Experiment Station Hatch Program (CRIS project number VA-135981). **Author contributions:** K.D.A., G.W., and R.H.W. designed the research. K.D.A., G.W., D.M.S., X.F., and R.H.W. performed the experiments. K.D.A., G.W., D.M.S., X.F., R.J.B., J.W., and R.H.W. analyzed and interpreted the data. K.D.A., G.W., D.M.S., X.F., and R.H.W. wrote the paper. All authors approved the final version of the manuscript. **Competing interests:** The authors declare that they have no competing interests. **Data and materials availability:** All data needed to evaluate the conclusions in the paper are present in the paper and/or the Supplementary Materials.

Submitted 8 February 2021
Accepted 8 September 2021
Published 27 October 2021
10.1126/sciadv.abg9739

Citation: K. D. Allen, G. Wegener, D. Matthew Sublett Jr, R. J. Bodnar, X. Feng, J. Wendt, R. H. White, Biogenic formation of amorphous carbon by anaerobic methanotrophs and select methanogens. *Sci. Adv.* **7**, eabg9739 (2021).

Science Advances

Biogenic formation of amorphous carbon by anaerobic methanotrophs and select methanogens

Kylie D. AllenGunter WegenerD. Matthew Sublett JrRobert J. BodnarXu FengJenny WendtRobert H. White

Sci. Adv., 7 (44), eabg9739. • DOI: 10.1126/sciadv.abg9739